SUBSONIC DYNAMIC STABILITY TESTS OF A SAMPLE RETURN ENTRY VEHICLE

C. Michael Fremaux[1] and R. Keith Johnson[2]

[1] Senior Research Engineer, Flight Dynamics Branch, MS 308, NASA Langley Research Center, Hampton, Virginia, U.S.A, 23681, c.m.fremaux@larc.nasa.gov

[2] Aerospace Engineer, Exploration Systems Engineering Branch, MS 489, NASA Langley Research Center, Hampton, Virginia, U.S.A, 23681, r.k.johnson@larc.nasa.gov

ABSTRACT

An investigation has been conducted in the NASA Langley 20-Foot Vertical Spin Tunnel (VST) to determine the subsonic dynamic stability characteristics of a proposed atmospheric entry vehicle for sample return missions. In particular, the effects of changes in aft-body geometry on stability were examined. Free-flying tests of a dynamically scaled model with various geometric features were conducted, including cases in which the model was perturbed to measure dynamic response. Both perturbed and non-perturbed runs were recorded as motion time histories using the VST optical data acquisition system and reduced for post-test analysis. In addition, preliminary results from a static force and moment test of a similar model in the Langley 12-Foot Low Speed Tunnel are presented. Results indicate that the configuration is dynamically stable for the baseline geometry, but exhibits degraded dynamic behavior for the geometry modifications tested.

1. SYMBOLS

C_m — body axis pitching moment

C_{mo} — zero-lift static pitching moment coefficient

$C_{m_{\hat{q}}} + C_{m_{\dot{\alpha}}}$ — sum of damping derivatives due to pitch rate and time rate of change of angle of attack, rad^{-1}

$\overline{C}_{m_{\hat{q}}}$ — pitch damping derivative; approximation of $C_{m_{\hat{q}}} + C_{m_{\dot{\alpha}}}$, rad^{-1}

d — model or vehicle maximum diameter, ft

I_{xx}, I_{yy}, I_{zz} — moment of inertia about model or vehicle x, y or z body axis, respectively, $slug\text{-}ft^2$

M — Mach number

m — mass, slugs

q — pitch rate about model y axis, rad/s

$\hat{q}$ — reduced pitch rate, $qd/2V$

$\overline{q}$ — free-stream dynamic pressure, $1/2\rho V^2$, lb/ft^2

r_n — nose radius, ft

r_{sa} — aft radius of shoulder, ft

r_{sf} — forward radius of shoulder, ft

Re — Reynolds number, $\rho V d/\mu$

S — reference area, $\pi d^2/4$, ft^2

t — full-scale time, s

V — full-scale sink rate, ft/s

X, Y, Z — coordinates in tunnel-fixed reference system, in

x, y, z — coordinates in model or vehicle body-fixed reference system, with x coincident with model axis of symmetry, in

α — true (aerodynamic) angle of attack, deg

$\dot{\alpha}$ — time rate of change of angle of attack, deg/s

$\overline{\alpha}$ — $\theta + 90$; approximately equal to model or vehicle angle of attack, deg

$\overline{\alpha}_T$ — total pitch angle calculated from model attitude time history estimates, deg

ϕ — roll angle; angle between y body axis and an arbitrary reference, measured in a horizontal plane, deg

μ — absolute viscosity, $lb\ sec/ft^2$

ρ — air density, $slugs/ft^3$

σ — standard deviation

θ — pitch angle; angle between x body axis and horizontal, measured in a vertical plane. Equals -90 for model or vehicle nose pointing straight down, deg

ψ   yaw angle; angle between y body axis and horizontal. Equals 0 for model or vehicle pointing straight down, deg

2. INTRODUCTION

2.1 Background

Several free-flying model tests were used to determine the dynamic behavior of a proposed sample return vehicle in vertical free-fall at terminal velocity. This vehicle concept enters the atmosphere passively without a parachute, which is typically used to provide deceleration and stability over the subsonic flight regime. Without a parachute, maintaining aerodynamic stability and proper orientation for landing is critical. The model was originally flown in the NASA Langley 20-Foot Vertical Spin Tunnel (VST) in its baseline configuration in 2004, and it was noted that its dynamic behavior was relatively benign compared to that of a generic model with a similar forebody shape [1] that had been tested in the late 1990s. Based on this difference in behavior, a second test entry was planned to help understand why the dynamic behavior of the current model was superior to that in [1]. Two backshell modifications were designed and fabricated for the current model in an attempt to emulate some of the geometric features of the earlier model [1]. It was hypothesized that these features might be promoting unsteady flow on the backshell, resulting in a dynamic instability. Re-running the tests with the modifications installed showed that they did influence the behavior of the current model by making it less dynamically stable, or even unstable (i.e., divergent) in some cases. In a related effort, static force and moment tests of a full-scale model were conducted in the Langley 12-Foot Low Speed Tunnel (12-Foot) to quantify the static stability characteristics of the configuration. The backshell modifications were also tested on the static model. Results from the VST test will be discussed in detail in a later section. Results from the 12-Foot test will be summarized and used to augment the analysis of the VST results where appropriate.

2.2 Wind Tunnel

The dynamic stability tests were performed in the Langley 20-Foot Vertical Spin Tunnel (VST). In operation since 1941, the VST is an atmospheric, low-speed, annular return tunnel with a closed, twelve-sided test section that is 20 feet across and 25 feet tall. A cross-sectional sketch of the facility is shown in Fig. 1. Maximum tunnel dynamic pressure ($\bar{q}$) is approximately 9 lb/ft^2 at a speed of 87 ft/s (Re = 0.55 x 10^6/ft, M = 0.08). Upper and lower nets prevent models from getting drawn into the fan or falling through the flow straightening "honeycomb", respectively. The test

section walls are padded to minimize model damage due to impact, but a "safety tether" was used during these tests in order to further reduce the likelihood of model damage and reduce downtime due to model repair. The tether consists of lightweight braided nylon line attached to the model with a ball-bearing swivel. It was kept slack during data runs, but was tightened to prevent impact by an operator using an electric winch if the model drifted near a wall. A series of cameras around the test section provide video coverage for visual documentation of the test as well as input to an optical data acquisition system (to be discussed in the next section). The VST has a long history of testing aircraft models, primarily for determining spin and spin-recovery characteristics, but there have been numerous dynamic stability and drogue parachute sizing tests for atmospheric entry vehicles over the years, including Mercury [2], Gemini [3], Apollo [4], Pioneer Venus [5] and several proposed planetary entry vehicles in addition to more recent tests of the Stardust [6] and the generic configuration previously mentioned.
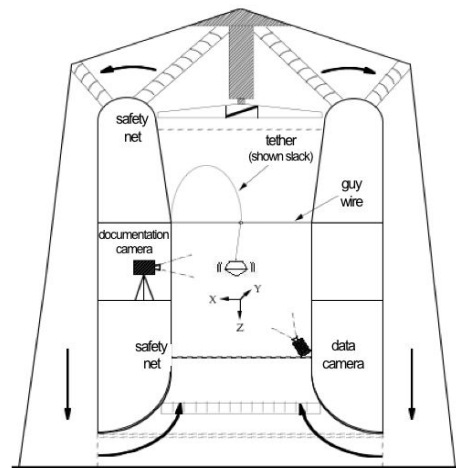

Fig. 1 Cross-section of 20-Foot Vertical Spin Tunnel

2.3 Data acquisition system

An optical data acquisition system is used to obtain 6 degree-of-freedom (6-DOF) motion time histories of models during dynamic tests. The VST Model Space Positioning System, or MSPS [7], is a non-intrusive, workstation-based system that uses three single-camera views of retro-reflective targets on a model to generate post-test estimates of model attitude (ψ, θ, ϕ) and spatial position (X, Y, Z) with respect to an earth-fixed test-section axis system (Fig. 1) at a sample rate of 60 Hz. At the start of data acquisition, test section state (dynamic pressure, flow velocity, temperature, etc.) is recorded on a separate system and time-correlated for post-test processing. Numerical differentiation of the attitude time histories is used to calculate angular rates. Comparisons to a reference at known attitudes indicate

that angles reported by MSPS are accurate to within ±1 degree.

2.4 Model

A 53%-scale model of the proposed sample return vehicle in the baseline configuration was fabricated at the NASA Langley Composite Model Shop using a rapid prototyping technique to significantly reduce cost and fabrication time compared to earlier sample return models tested in the VST (e.g., [1], [6]). A sketch of the geometric features of the baseline configuration is shown in Fig. 2, and a photo of the model flying in the VST is shown in Fig. 3.
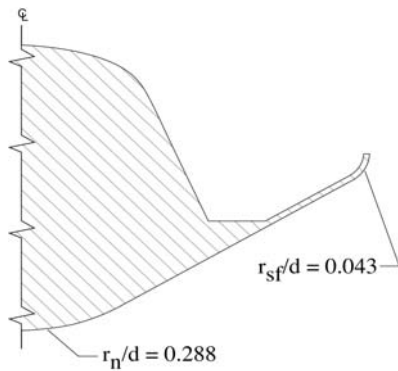

Fig. 2. Baseline configuration geometric features

Fig. 3. 53%-scale sample-return model in the VST

The vehicle features a spherically-blunted cone forebody with a 60-degree half angle and a nose radius that is 28.8% of the maximum (base) diameter (note that the model referred to in [1] had a slightly different nose radius of 25%, and is referred to as the "6025" model in that paper). The model was ballasted (using lead weights) to achieve model-to-vehicle similitude of inertial and gravitational forces using the dynamic scaling laws [8] (i.e. maintaining constant Froude number and vehicle-to-atmosphere relative density factor). For a dynamically scaled model, not only are the geometric characteristics similar to the full-scale vehicle, but the mass, center of gravity (c.g.) and

moments of inertia are scaled as well. Adherence to the dynamic scaling laws allows direct conversion of the model linear and angular rates to full-scale, with the assumption that Reynolds number (Re) and Mach number (M) effects are not significant. For the 53% scale model, the factor for converting time from model-scale to full-scale is approximately 1.37, i.e., rates during the model tests are 1.37 times faster than full-scale.

Two modifications to the backshell were also fabricated as "appliqués" that could be attached to the model. These modifications were designed to approximate some of the backshell features of the 6025 model tested in [1]. The first modification (Mod 1) consisted of a ring that covered the sharp rear-facing corner of the forebody-backshell juncture with a relatively large radius shoulder (Fig. 4). The second modification (Mod 2) used the same radius shoulder as Mod 1 but faired it into a flat plate that covered the concave portion of the backshell (Fig. 5).
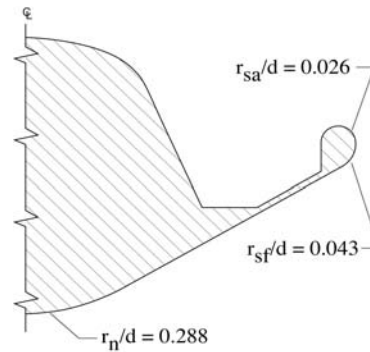

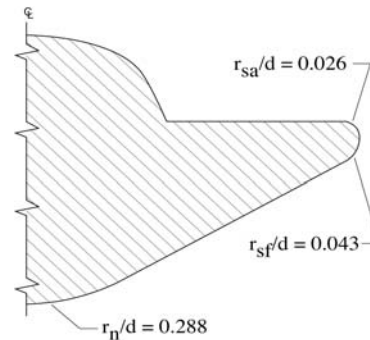**Fig. 4. Mod 1 geometric features (shoulder installed)**

Fig. 5. Mod 2 geometric features (shoulder + backplate installed)

Regardless of configuration, the model was ballasted to obtain dynamic similarity to the full-scale entry vehicle at an altitude of 5000 ft ($\rho = 2.04 \times 10^{-3}$ slug/ft^3 based on the 1976 Standard Atmosphere [9]). The target mass, moments of inertia (MOI), and center of gravity location used during the dynamic test (based on the full-scale vehicle) appear in Table 1.

Table 1. Full-Scale Mass Properties of Proposed Sample-Return Vehicle

parameter	target value	comment
m	0.795 slugs	
Ixx	0.143 slug-ft^2	roll MOI
Iyy	0.098 slug-ft^2	pitch MOI
Izz	0.099 slug-ft^2	yaw MOI
c.g. location	0.23d	x = 5.198 inches aft of nose and on axis of symmetry (y = 0, z = 0)

Model mass properties were measured prior to testing (and any time the model configuration was changed) on a "swing rig" [10]. The accuracy of the mass property measurements (based on calibration standards traceable to National Institute of Standards) is summarized in Table 2.

Table 2. Accuracy of Mass Property Measurements

parameter	accuracy
m	± 0.1%
Ixx	.± 0.25%
Iyy	.± 0.25%
Izz	.± 0.25%
c.g.	± 0.001d

2.5 Test technique

For the dynamic model tests, the model was "free-flying" in the tunnel (with the exception of lightweight tether described in section 2.2). For each test run, the model was attached to the tether and lowered into the test section. Any residual movement of the model was damped out with a long-handled hook that can grasp the tether anywhere along its length. The tunnel operator brought the test section velocity up to a point where the weight was taken off of the tether and the model was free-flying (i.e., model average drag equals model weight). A technician ensured that the tether was kept slack by making adjustments to the electric winch if required. Once the model was stabilized in the test section, the MSPS data acquisition system was activated for a pre-determined amount of time to capture the motion of the model. The length of each data record was dependent on the amount of time the model stayed

in the field of view of the MSPS cameras, and is thus variable from run to run. In some cases, the technician perturbed the model by striking one side with the hook so as to cause the model to oscillate. While there is no way to precisely control the amount of initial displacement, efforts were made to be as consistent as possible. Both types of tests (perturbed and non-perturbed) were conducted for all of the model configurations (baseline, Mod 1, and Mod 2).

3. RESULTS AND DISCUSSION

3.1 Motion time histories

Several runs were made for each combination of model geometry and test type (i.e., perturbed or non-perturbed). Time history plots of total pitch angle ($\bar{\alpha}_T$), with the model results converted to full-scale, are presented in this section. In this paper, a representative run for each combination will be presented to save space. While variations in model dynamics existed run-to-run, the overall character was generally similar and thus useful for comparing and contrasting the behavior resulting from geometric changes. The time history plots in the next section are plotted as continuous curves instead of discreet data points for clarity. The scale of the vertical axes was chosen to accommodate the largest amplitude oscillations observed and thus highlight differences among the results. The length of the time scales (horizontal axes) was allowed to vary depending on the length of the data record. Periodically, the MSPS loses track of a model due to occlusion of the targets or glints on the model that confuse the system. Loss of track by MSPS is reflected as gaps in the curves. An unbroken line indicates that the system tracked at the full 60 Hz (model scale) sample rate.
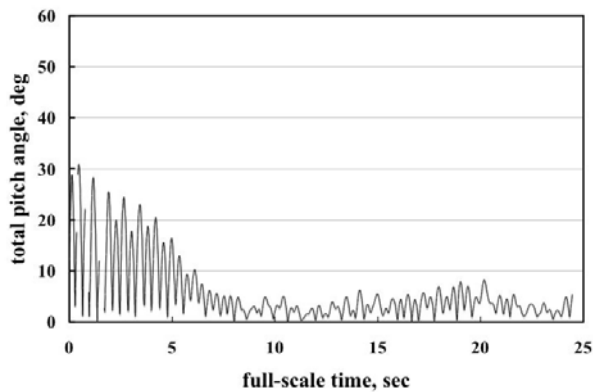
3.1.1 Baseline configuration

Results for the baseline configuration appear in Fig. 6 (unperturbed) and Fig. 7 (perturbed). For the unperturbed run, the total pitch angle ($\bar{\alpha}_T$) is seen to vary in a "limit cycle" oscillation. This type of behavior is typical of blunt entry vehicles at subsonic conditions. Note that compared to "classic" limit-cycle behavior in aircraft flight dynamics (such as wing rock), the cycle-to-cycle peak amplitude varied significantly with time. While wing rock is primarily a 1-DOF motion about an airplane's roll axis, axisymmetric blunt-bodies tend to oscillate about the pitch and yaw axes simultaneously, often in a pattern that prevents both the pitch and yaw angles from crossing through zero. Small disturbances (such as variations in test section flow field) can trigger the initial oscillations, but they are often self perpetuating due to the aerodynamic behavior of a particular vehicle (e.g., statically stable but marginal or

even negative dynamic damping near zero angle of attack). The peak amplitude reached during the run as about 11 degrees, but was significantly less than 10 degrees for most of the run.
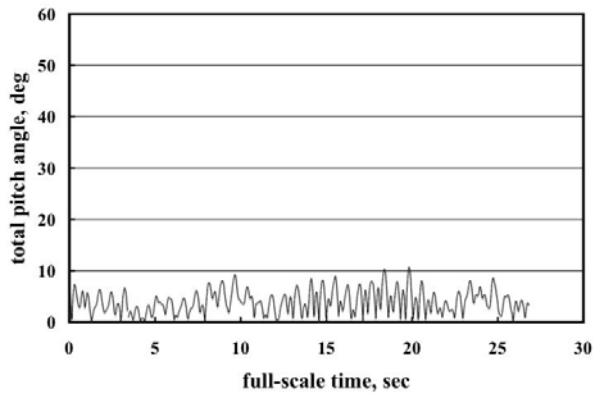
Fig. 6. Baseline configuration, unperturbed

When perturbed, the baseline configuration exhibited clear damping, as illustrated in Fig. 7.
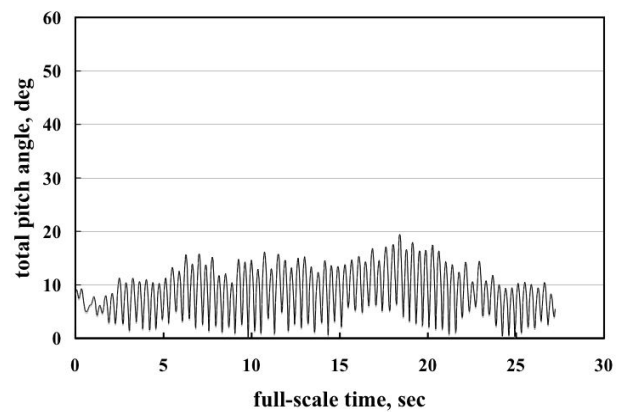

Fig. 7. Baseline configuration, perturbed

The MSPS began sampling just after the model heeled over, with an initial displacement near 30 degrees. A near-linear reduction in cycle-to-cycle amplitude is evident for the first five seconds, with a steeper drop thereafter until a limit cycle is established at between seven and eight seconds. This is in contrast to the results from [1], in which limit-cycle amplitudes in the range of 25 to 30 degrees were sustained after perturbation, with no evidence of decay during the run. Note that the model in [1] was ballasted to the same c.g. location. This difference in behavior was the motivation for examining the effect of geometry modifications to the current model (Mod 1 and Mod 2), to be presented in the next section.
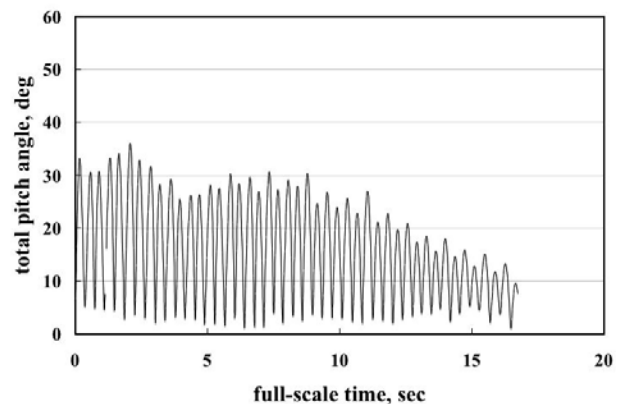
3.1.2 Mod 1 configuration

As noted earlier, the Mod 1 configuration consisted of a ring that was installed over the relatively sharp

forebody-backshell juncture of the baseline configuration. It was postulated that installing a large radius shoulder similar to that used in [1] might promote attached flow on the backshell, in contrast to the sharp trailing edge of the baseline configuration, which likely forces the flow to separate cleanly. In Fig. 8, the results for the unperturbed model are shown. In contrast to the baseline, the amplitude of the limit-cycle rocking is significantly larger, with the total pitch angle varying between about 10 degrees and 17 degrees during most of the run (with one spike of nearly 20 degrees). Since the mass properties, test conditions, and geometric features (other than the rounded shoulder) of the Mod 1 test were similar to that of the baseline, the different dynamic behavior appears to be caused by the difference in geometry.

Fig. 8. Mod 1 (shoulder added) configuration, unperturbed

When the Mod 1 was perturbed (Fig. 9), the steep drop off in amplitude noted for the baseline is not evident, even though the initial displacements were similar (about 32 degrees in this case).

Fig. 9. Mod 1 (shoulder added) configuration, perturbed

In fact, the amplitude tended to grow for over several cycles before beginning to decay. A second interval of growth is noted before the oscillation envelope begins a final gradual decay. In this case, the run ended prior to a

clear limit cycle being re-established, but the final amplitude is within the range displayed in Fig. 8. As with the unperturbed results, changing the sharp, aft-facing corner to a relatively large-radius shoulder appears to have affected the dynamic response of the model in otherwise similar test conditions.

3.1.3 Mod 2 configuration

The Mod 2 configuration added a flat plate, or disk, to the back of the model (faired into a corner with the same radius as the Mod 1 shoulder) that covered the concave backshell of the model. This configuration was the most similar (in terms of outer mold line) to the 6025 model in [1]. When perturbed only by the tunnel flow, the model exhibited limit-cycle behavior that displayed features noted in the previous two cases, i.e., alternating periods of relatively large amplitudes of up to 13 degrees and oscillations in the 5 degree range (Fig. 10).
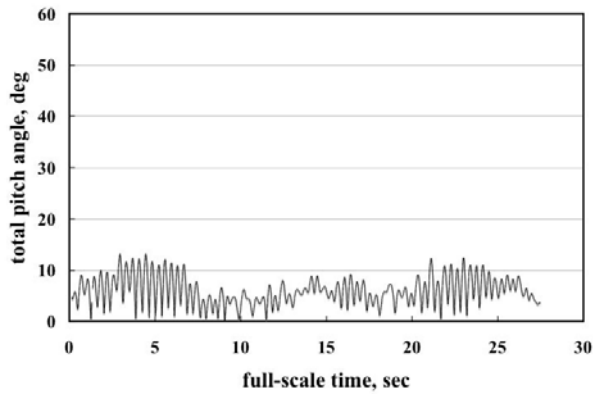

Fig. 10. Mod 2 (shoulder + backplate added) configuration, unperturbed

When the Mod 2 was perturbed (Fig. 11), the behavior of the model was significantly more dynamic than in the earlier cases.
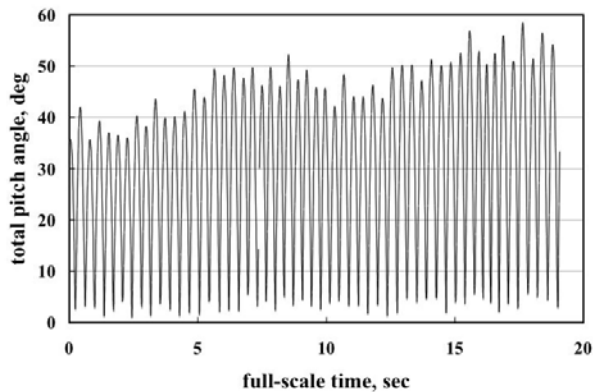

Fig. 11. Mod 2 (shoulder + backplate added) configuration, perturbed

3.2 Static and dynamic stability estimates

The initial perturbation of about 35 degrees (~3 degrees more than the Mod 1 case) resulted in the model entering a divergent oscillation. While the peak values of $\overline{\alpha}_T$ grew or decayed cycle-to-cycle, the overall trend was a clear growth in the oscillation envelope. The peak value reached near the end of the test record was nearly 60 degrees. While the model did not flip over during the test, other models (e.g., [1], [6]) did begin tumbling soon after reaching pitch angles of this magnitude. It is possible that longer test times would have allowed the amplitude to build up to a point that the model pitch angle diverged.

As mentioned earlier, a static force and moment test was conducted in the Langley 12-Foot Low Speed Tunnel on a full-scale model, including the Mod 1 and Mod 2 configurations. The static stability level of the vehicle will be estimated from the results of the 12-Foot test. Likewise, a measurement of dynamic stability (in a linear sense) is the pitch damping derivative $\overline{C}_{m_{\dot{q}}}$. Pitch damping will be estimated from the time histories that were presented in section 3.1

3.2.1 Static stability

A plot of pitching moment coefficient (resolved about the vehicle target c.g. location 0.23d aft of the nose and on the axis of symmetry) for all three configurations appears in Fig. 12. These data were taken at a dynamic pressure ($\overline{q}$) of 2 psf ($Re_d \approx 0.49 \times 10^6$). In contrast, the dynamic pressure during the VST tests was on the order of 6 psf, but due to the 53% scale of the dynamic model relative to the (full-scale) model tested in the 12-Foot tunnel, the Reynolds number based on maximum diameter (d) during the two tests was approximately the same.
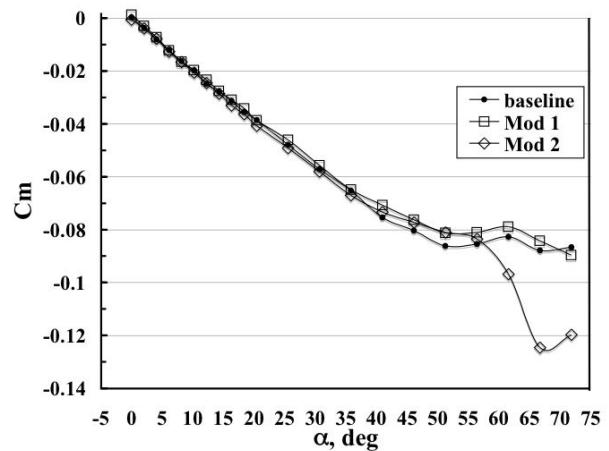

Fig. 12. Pitching moment coefficient from 12-Foot Low Speed Tunnel tests

Though there are slight variations in pitching moment coefficient for a given angle of attack among the three

configurations, the curves are quite similar and linear to angle of attack of 35 degrees. Arbitrarily choosing an angle of attack range of 0 to 8 degrees and calculating the slope results in the static stability estimates ($C_{m\alpha}$) shown in Table 3. Note that negative values of $C_{m\alpha}$ indicate static stability.

Beyond α=50 degrees, the pitching moment characteristics of all three configurations become non-linear, with the baseline and Mod 1 experiencing moderate unstable breaks (i.e. change in slope from negative to positive), while Mod 2 exhibits a very large stable break at 55 degrees before again breaking unstable at about 67 degrees. This large stable break likely is a driving force in the large amplitude oscillations noted in Fig. 11, i.e., Mod 2 has a stiffer "spring" to force the vehicle toward lower angles of attack. If this stiff static system is coupled with very small (or even negative) damping, dynamic motions may exhibit limit-cycle or divergent oscillations. Presumably, the ability of the flow to "turn the corner" and remain attached to the backshell (due to the presence of a large-radius corner coupled with a flat, surface) was the driver for the significantly different pitching moment characteristics exhibited by Mod 2 at large angles of attack. The large-radius corner of the Mod 1 configuration did not have a significant impact on the static pitching moment relative to the baseline. It is likely that the large turning angle due to the concave backshell prevented extensive flow attachment in spite of the presence of the shoulder.

It should be noted that the 12-Foot tests were conducted using pitch sweeps that progressed from the low to high angles of attack, but did not take data as the angle of attack was reduced from maximum. Therefore, it is not known if static hysteresis is present in the pitching moment characteristics of any of the configurations examined. Static hysteresis has been linked to the aircraft wing rock phenomenon (e.g., [11]) and could be a driver for the motions observed during the present dynamic tests.

Table 3. Static Stability Parameter Estimates
(12-Foot LST data; slope computed between $\alpha=0^{o}$ and $\alpha=8^{o}$)

configuration	$C_{m\alpha}$, deg^{-1} (static test)
Baseline	-0.116
Mod 1	-0.124
Mod 2	-0.112

3.2.2 Dynamic stability

The time histories of Figs. 7, 9, and 11 were used to estimate the dynamic damping-in-pitch ($\overline{C}_{m_{\hat{q}}}$) of the three configurations. Two different methods were used to extract approximations of this parameter as outlined next.

A simple hand calculation can be performed to get an initial assessment of pitch damping. With some simplifying assumptions, the 1-DOF pitch equation of motion

$$C_{m_{total}} = C_{m_o} + C_{m_\alpha}\alpha + \overline{C}_{m_{\hat{q}}}\hat{q} = \frac{Iyy}{\overline{q}Sd}\ddot{\theta}\quad(1)$$

(i.e., a classic spring-mass-damper system) can be used to calculate the total (i.e., static-plus-dynamic) aerodynamic pitching moment from the calculated angular acceleration and dynamic pressure during a test, measured MOI, and model reference area and diameter. Calculating the $\Delta C_m/\Delta\hat{q}$ at a given angle of attack for the positive and negative pitch rate during each cycle and averaging over several cycles gives an estimate for $\overline{C}_{m_{\hat{q}}}$. For the present work, motion time histories from Figs. 7, 9, and 11 were used with Eq. 1 to calculate the total pitching moment value each time the model crossed α=0 (noting that α=θ due to kinematics associated with the 1-DOF motion assumption). Since the model is axisymmetric, the static aerodynamic contribution to the total pitching moment vanishes at zero angle of attack and any non-zero pitching moment is assumed to be a function of angular rate only. These C_m values were plotted against their respective positive or negative $\hat{q}$ values to calculate $\Delta C_m/\Delta\hat{q}$ for each half cycle of the oscillation. Regardless of the configuration, the pitch damping estimated using this method was on the order of -0.35, which indicates significant damping. Based on the different dynamic responses for the three configurations noted in Figs. 7, 9, and 11, it is clear that a single-point estimate at α=0 is not adequate to describe the damping characteristics of the vehicle if there is appreciable deviation from α=0. It is likely that damping varies widely with angle of attack during an oscillation cycle.

The second method used involved the use of a parameter identification (PID) technique. The SIDPAC [12] software package consists of a suite of MATLAB® scripts for modeling flight data and extracting aerodynamic coefficients. Again assuming 1-DOF and a linear model of the aerodynamic coefficients (i.e., Eq. (1)), the three time histories were run through a 1-DOF aerodynamic extraction program built using SIDPAC. While assuming a constant value of pitch damping is likely not adequate to fully model the motion (as there may be linear or even non-linear dependencies on angle of attack, amplitude, rates, etc.) it is reasonable to start

with a linear model before moving to more complex models. The PID approach used here calculates a single value of $\overline{C}_{m_{\dot{q}}}$ that best represents the response (within the limitations of the linear model) over the entire range of motion, not just a single point. A sample of the modeling results is shown in Fig. 13, where pitching moment coefficient is plotted versus time. Input for this calculation was a truncated version of Fig. 7 with only the cycles of clearly decreasing amplitude retained.
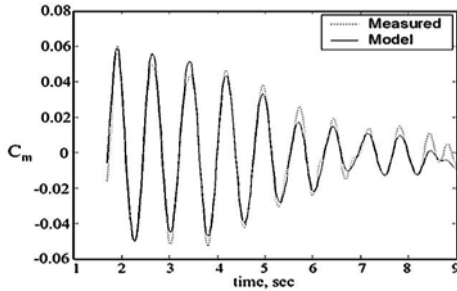
Fig. 13. Pitching moment coefficient from 20-Foot VST test using PID technique for baseline configuration

The "Measured" curve (dashed line) represents the total (1-DOF) pitching moment calculated directly from the RHS of Eq. (1). The "Model" curve (solid line) represents the linear buildup of the estimated aerodynamics from SIDPAC, which does a reasonable job of capturing the overall character of the motion, but misses the peak values (overshooting or undershooting) for several of the cycles. Average damping derivative estimates for the three configurations are presented in Table 4, along with the 2σ (95% confidence) bounds from SIDPAC. Also in Table 4 are the estimated values of static stability, $C_{m\alpha}$, based on the PID modeling. Note that the static stability levels from the 12-Foot test (Table 3) and VST test are in reasonable agreement.

In Table 4, there is a clear progression from damped (-.047) for the baseline, to near neutral dynamic stability (-0.007) for Mod 1, to slightly propelling (+0.008) for Mod 2. The trend in these results is in agreement with the that observed for the three configurations.

Table 4. Static and Dynamic Stability Parameter Estimates
(PID estimates from 20-Foot VST time histories)

Configuration	$C_{m\alpha}$, deg^{-1} (from dynamic tests)	$\overline{C}_{m_{\dot{q}}}$, rad^{-1} (+/- 2σ)
Baseline	-0.137	-0.047 +/-0.018
Mod 1	-0.132	-0.007 +/-0.018
Mod 2	-0.137	+0.008 +/-0.009

4. CONCLUSIONS

1. The baseline configuration, at the center of gravity location and scaled mass properties of the test, will be statically and dynamically stable at low mean angles of attack, with a limit-cycle amplitude of 10 degrees or less.

2. Excursions in total angle of attack as large as 30 degrees will damp out to a small-amplitude limit cycle once the excitation causing the excursions ceases.

3. Differences in aft-body geometry, notably the sharpness or bluntness of the forebody to aft-body juncture and the total turning angle created by the corner will affect the level of pitch damping, possibly resulting in a dynamically unstable configuration.

4. Oscillatory motion over an appreciable angle of attack range will not be adequately described using a single-point estimate of pitch damping at α=0, but can be modeled reasonably well using a pitch damping value that is estimated while taking the entire range of motion into consideration.

5. REFERENCES

1. Mitcheltree, R. A., Fremaux, C. M., and Yates, L. A., Subsonic Static and Dynamic Aerodynamics of Blunt Entry Vehicles, AIAA 99-1020, 1999.

2. Bowman, J. S., Dynamic Model Tests at Low Subsonic Speeds of Project Mercury Capsule Configurations with and without Drogue Parachutes, NASA TM X-459, 1961.

3. Bowman, J. S., Dynamic-Model Investigation of a 1/20-Scale Gemini Spacecraft in the Langley Spin Tunnel, NASA TN-D-2191, 1964.

4. Lee, H. A., and Burk, S. M., Low-Speed Dynamic Model Investigation of Apollo Command Module Configurations in the Langley Spin Tunnel, NASA TN-D-3888, 1967.

5. McCloy, R., Entry Dynamics Performance Predictions for Pioneer Venus Probes, AIAA-1978-1370, 1978.

6. Mitcheltree, R. A. and Fremaux, C. M., Subsonic Dynamics of Stardust Sample Return Capsule, NASA TM 110329, 1997.

7. Snow, W. L., Childers, B. A., Jones, S. B., and Fremaux, C. M., Recent Experiences with Implementing a Video Based Six Degree of Freedom Measurement System for Airplane Models in a 20-Foot Diameter Vertical Spin Tunnel, *Proceedings of the SPIE Videometrics Conference*, Vol. 1820, 1992, pp. 158-180.

8. Wolowicz, C. H., Bowman, J. S., and Gilbert, W. P., Similitude Requirements and Scaling Relationships as Applied to Model Testing, NASA TP 1435, 1979.

9. United States Committee on Extension to the Standard Atmosphere: *U.S. Standard Atmosphere*, 1976.

10. Boynton, R., and Wiener, K., A New High Accuracy Instrument for Measuring Moment of Inertia and

Center of Gravity, Society of Allied Weight Engineers SAWE Paper No. 1827, 1988.

11. Nguyen, L., Yip, L., and Chambers, J., Self-Induced Wing Rock of Slender Delta Wings, AIAA 81-1883, 1981.

12. Morelli, E., System IDentification Programs for AirCraft (*SIDPAC*), AIAA paper 2002-4704, 2002.